Localized Flux Maxima of Arsenic, Lead, and Iron around Root Apices in Flooded Lowland Rice

Williams, P. N., Santner, J., Larsen, M., Lehto, N. J., Oburger, E., Wenzel, W., ... Zhang, H. (2014). Localized Flux Maxima of Arsenic, Lead, and Iron around Root Apices in Flooded Lowland Rice. Environmental Science and Technology, 48(15), 8498-8506. DOI: 10.1021/es501127k

Published in:
Environmental Science and Technology

Document Version:
Publisher's PDF, also known as Version of record

Environmental Science & Technology

Article

pubs.acs.org/est

Localized Flux Maxima of Arsenic, Lead, and Iron around Root Apices in Flooded Lowland Rice

Paul N. Williams,*[,†,‡] Jakob Santner,[§] Morten Larsen,[∥,⊥,#] Niklas J. Lehto,[†,¶] Eva Oburger,[§] Walter Wenzel,[§] Ronnie N. Glud,[∥,⊥,#,▽] William Davison,[†] and Hao Zhang[†]

[†]Lancaster Environment Centre, Lancaster University, Lancaster LA1 4YQ, United Kingdom

[‡]Institute for Global Food Security, Queen's University Belfast, Belfast BT9 5HN, United Kingdom

[§]Rhizosphere Ecology and Biogeochemistry Group, Institute of Soil Science, Department of Forest and Soil Sciences, University of Natural Resources and Life Sciences, Konrad-Lorenz-Straße 24, A-3430 Tulln, Austria

[∥]Institute of Biology and Nordic Centre for Earth Evolution (NordCEE), University of Southern Denmark, 5230 Odense M, Denmark

[⊥]Greenland Climate Research Centre, Greenland Institute of National Resources, Kivioq 2, Post Office Box 570, 3900 Nuuk, Greenland

[#]Scottish Marine Institute, Scottish Association for Marine Science, Oban PA37 1QA, United Kingdom

[¶]Faculty of Agriculture and Life Sciences, Lincoln University, Post Office Box 84, Lincoln 7647, New Zealand

[▽]Arctic Research Center, Arhus University, 8000 Aarhus C, Denmark

Supporting Information

ABSTRACT: In wetland-adapted plants, such as rice, it is typically root apexes, sites of rapid entry for water/nutrients, where radial oxygen losses (ROLs) are highest. Nutrient/toxic metal uptake therefore largely occurs through oxidized zones and pH microgradients. However, the processes controlling the acquisition of trace elements in rice have been difficult to explore experimentally because of a lack of techniques for simultaneously measuring labile trace elements and O_2/pH. Here, we use new diffusive gradients in thin films (DGT)/planar optode sandwich sensors deployed *in situ* on rice roots to demonstrate a new geochemical niche of greatly enhanced As, Pb, and Fe(II) mobilization into solution immediately adjacent to the root tips characterized by O_2 enrichment and low pH. Fe(II) mobilization was congruent to that of the peripheral edge of the aerobic root zone, demonstrating that the Fe(II) mobilization maximum only developed in a narrow O_2 range as the oxidation front penetrates the reducing soil. The Fe flux to the DGT resin at the root apexes was 3-fold higher than the anaerobic bulk soil and 27 times greater than the aerobic rooting zone. These results provide new evidence for the importance of coupled diffusion and oxidation of Fe in modulating trace metal solubilization, dispersion, and plant uptake.

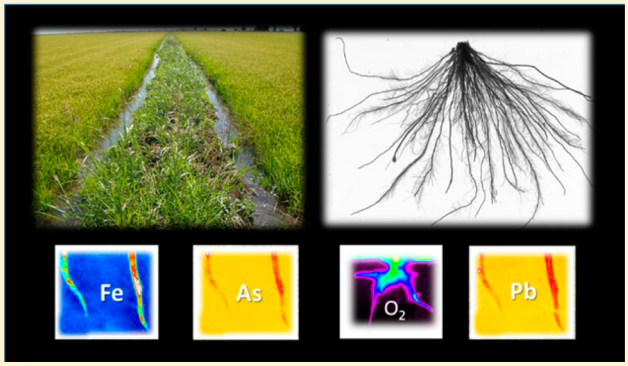

INTRODUCTION

Rice contains ~10 times more arsenic than other cereal staples[1] and is the dominant food source of inorganic arsenic exposure to the world's population.[2,3] The prevalence of lead-enriched rice is less than that of arsenic but is a particular concern in regions where waste recycling and base metal mining coexist with farming.[4] Lead exposure is estimated to be responsible for 0.6% of the global burden of disease.[5] When rice is consumed in quantity, representing the eating habits of many in southeast Asia, by children or expectant mothers, its contribution to critical exposure levels can be significant.[4] Conversely, it is the sub-optimum concentrations of iron in polished rice that contribute to iron deficiency, the most common human micronutrient imbalance in the world.[6] However, despite this, iron toxicity is one of the most devastating trace element disorders in lowland rice, inhibiting the uptake and use of essential nutrients.[7] Plant uptake of arsenic, lead, and iron is influenced strongly by soil processes and root activities, but our understanding of related mobilization/immobilization of those elements in rice rhizospheres remains incomplete because of the lack of satisfactory biogeochemical *in situ* mapping technologies.

Received: March 6, 2014
Revised: June 25, 2014
Accepted: June 26, 2014
Published: June 26, 2014

   dx.doi.org/10.1021/es501127k | Environ. Sci. Technol. 2014, 48, 8498−8506

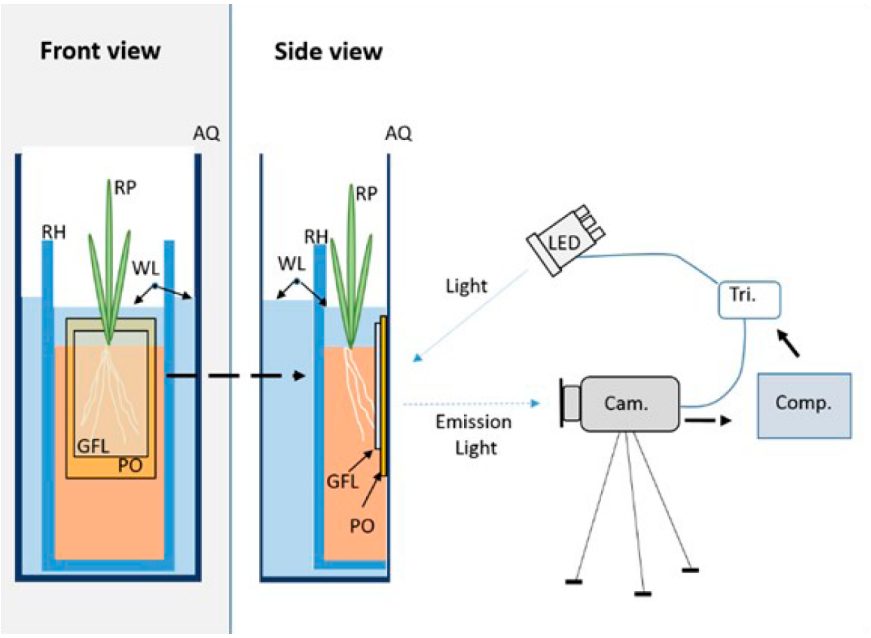

Figure 1. Scheme of the experimental design. Illustrated within the diagram is the rhizotron (RH), planar optode (PO), ultrathin resin gel and filter layer (GFL), aquarium (AQ), rice plant (RP), camera (Cam.), trigger box (Tri.), light-emitting diode (LED), and computer (Comp.). The water level in both the rhizotron and aquarium is denoted by WL. The diagram is not to scale.

Soil-grown rice plants have a heterogeneous distribution of iron "plaque" coatings on their roots.[8,9] This discontinuous porous layer of amorphous oxyhydroxide minerals, believed to be composed of predominantly ferrihydrite,[10] on the root surface possesses a high specific surface area laden with −OH functional groups capable of reacting with metals, other cations, and anionic species.[11] Studies have shown that root iron plaques inhibit Cu, Ni, Mn, and P uptake in plants,[12−14] but given the right conditions, whereby Fe oxyhydroxide is reduced and recycled back into solution, they can also act as a source of supply.[8,15] The occurrence of iron plaques is more common around mature roots away from root tips.[9,16] As redox potentials decrease with rooting depth, this is matched by a decline in iron plaque formation.[16] Locations along the root axis where O_2 diffusion changes with time, coupled with the localized (bio)chemical ambience, will affect iron plaque formation. Because iron plaque is a strong sorbent for As and Pb, it is thought to retain these contaminants and render them unavailable for plant uptake. With this being the case, then root locations without dense plaque cover are considered entry points of As and Pb into the rice plants.

Flooding soil has a profound impact on the biogeochemical cycles of major and trace elements, primarily through influencing the reduction−oxidation (redox) reactions and altering pH.[17] It is frequently observed that iron mobilization in flooded soil is accompanied by concurrent release of arsenic.[18−21] It is the inorganic arsenic species, arsenate, that is central to arsenic mobilization upon soil flooding, by either it being liberated into solution as the host phase, iron oxide/hydroxide, is reduced or its (bio)chemical conversion to arsenite. The reduced species, arsenite, being less strongly bound to iron, is more inclined to partition into solution.[19,21] Once dissolved, the arsenate can be rapidly reduced biotically or abiotically for assimilation by rice. Lead is considerably less mobile than arsenic. It is chemisorbed on clays and oxides and complexed with organic matter and exhibits an increase in solubility as pH declines.[22] All of these processes occur under pronounced spatial and temporal heterogeneity within the radial extension of the rhizosphere.

In addition to variability in redox conditions, localized changes in soil pH would also have a bearing on iron plaque development/cycling. Biotic processes, such as the secretion of root exudates[23] or the release of H^+ from the roots to balance excess intake of cations over anions,[24] are the common focus of root-mediated pH change.[23] However, abiotic processes may be equally as significant. The potential importance of pH-mediated Fe(II) mobilization, caused by the oxidation of Fe(II) by O_2 was first recognized 2 decades ago in theoretical models of flooded soil.[25] Evidence of localized acidification and banding of Fe(III) with proximity to rice roots was later shown experimentally in averaged one-dimensional measurements.[24,26] The sampling approach, advanced as it was at the time, could only partially validate the Fe(II) solubility phenomena, because the Fe(II) maxima could not be directly observed because the measurements were not obtained *in situ*. Furthermore, these studies were unable to observe the accompanying mobilization of other elements, such as arsenic and lead. Methodologies that can simultaneously capture these changes to decipher the underlying geochemical processes around rice roots have until now not been available. However, recent developments in chemical imaging techniques[27−29] have enabled this study to report the first direct measurements of O_2 and H^+ concentrations along with the mobilization of Fe(II) and other trace metals, at a two-dimensional planar interface in rice rhizospheres.

The overall aim of the work was to determine whether metal mobilization is a common feature of rice rhizospheres and to establish the key processes controlling element release. To achieve this, we used new sandwich sensor technologies, consisting of planar optodes using O_2 and pH-sensitive luminophores, overlain by an ultrathin (70 μm) diffusive gradients in thin films (DGT) layer for measuring metals.[28]

dx.doi.org/10.1021/es501127k | *Environ. Sci. Technol.* 2014, 48, 8498−8506

MATERIALS AND METHODS

Method Summary. An ultrathin DGT layer is exposed to the soil and backed by a planar optode. It accumulates metals on a small particle size (0.2 μm) chelating resin and records directly the locally induced flux of trace metals during the entire deployment.[28−30] The planar optode resolves the O_2 concentrations or pH dynamics in near real time at a temporal resolution of 30 min.[27] For the same locations, two-dimensional images of metals, analyzed by inductively coupled plasma−mass spectrometry (ICP−MS) after laser ablation, and either O_2 or pH could be resolved with a spatial resolution of ∼100 μm. Both Fe(II) and Fe(III) are accumulated, but calculations using the speciation code WHAM[31] indicated that Fe(III) would be negligible at the applied conditions, because of the low solubility of $Fe(OH)_3$. Arsenic binds quantitatively to iminodiacetic chelating resins in the presence of iron. For the ratio of accumulated As and Fe(II) observed in this work, the accumulation of As is unaffected by the amount of accumulated iron.[32]

The sensors were deployed in purpose-built rice rhizotrons designed to simulate natural anaerobic conditions encountered in the field. The rhizotron was transferred into an aquarium, and the front window of the rhizotron was removed to enable contact of the combined sensor with a Nuclepore membrane (0.2 μm pore size and ∼10 μm thickness) support that overlaid the root and soil surface. Ingress of O_2 into the anaerobic soils was minimal because this operation was performed in aquarium water that had previously been deoxygenated with nitrogen. The planar optode foil was attached with tape (Scotch super 33+) to the support membrane and, subsequently, was overlain by the ultrathin resin gel and filter layer (GFL), which was also fixed with tape (Figure 1).

Seed Germination. Rice seeds (RIL 46) were sterilized in 0.5% NaOCl for 10 min and rinsed 3 times with deionized water. Seeds were soaked in deionized water overnight and then germinated at 25 °C for 2 days. Seedlings were transferred to a nylon net floating on $^1/_2$ strength Hoagland's solution, in a greenhouse (12 h photoperiod with a light intensity of 379 ± 89 W m^{-2}, day/night temperatures of 26.5 ± 2.4 and 20.2 ± 1.5 °C, respectively, CO_2 concentration of 743 ± 31 mg/m^3, and relative humidity of >70%). The experimental campaign consisted of four components: Experiments 1 and 2 targeted the rhizospheres of rice seedlings. The first partnered oxygen with metal measurements, and the latter partnered pH and metals. Experiment 3 was conducted without a plant, to ascertain the heterogeneity of the soil. In experiment 4, abiotic conditions of the rhizophere were simulated with an artificial root. In the oxygen optode experiments (experiment 1), the rice was grown hydroponically for 2 weeks prior to transplanting into the rhizotrons for a further 2 weeks. Transfer of rice into the rhizotron soil was performed after 5 days in the pH study (experiment 2), and the plants left to grow for 3 weeks before sensor deployment.

Preparation of Rhizotrons. Perspex rhizotrons with detachable front plates[29] (inner dimensions of $H \times W \times D$ = 40 × 10 × 1.5 cm) were filled with pre-moistened (∼10%, wt/wt), sieved (<2 mm) A-horizon Cambisol with a pH_{CaCl_2} of 5.4, and fine loam texture [1.7% Fe, 20 mg of Pb kg^{-1} from aqua regia digestion, and <2 mg of As kg^{-1} measured by X-ray fluorescence (XRF)], which was tamped in layers to achieve a homogeneous soil structure with a consistent bulk density of 1.3 kg L^{-1}. Soils were saturated evenly using a water feed system,[29] to enable the placement of Nuclepore membranes (0.2 μm pore size and ∼10 μm thickness). The membrane ensures that soil uniformity was maintained during sandwich sensor deployment and avoided disturbance to roots and soil when the perpex covering window was removed. Seedlings (RIL 46) were transplanted in close proximity to the front plate of the rhizotron. Roots were encouraged to develop alongside the membrane by setting the rhizotrons at an inclination of 30−45°. In each case, the rooting/soil zones were kept in darkness to avoid exposing the roots and associated soil to light, which could affect the root development and induce microphytic growth. Control (unplanted) systems accompanied planted experimental setups.

Optode Sensor Fabrication. The oxygen quenchable luminophore platinum(II)-5,10,15,20-tetrakis(2,3,4,5,6-pentafluorphenyl)-porphyrin (PtTFPP, http://www.frontiersci.com/) was chosen as an oxygen indicator.[33] PtTFPP and an antenna dye (coumarin C545, https://www.sigmaaldrich.com/) were mixed in a 1:2% (w/w) ratio, respectively, and dissolved in 4% (w/w) polystyrene using dichloromethane as the solvent.

For the pH-sensitive optode, the lipophilic 8-hydroxy-1,3,6-pyrenetrisulfonic acid trisodium (HPTS) indicator was chosen.[27,34] HPTS and an antenna dye (Macrolex yellow coumarin, http://www.simon-und-werner.de/) were mixed in a 1.5:1.5% (w/w) ratio, respectively, and dissolved in 10% (w/w) polyurethane hydrogel (Hydromed D4) in a 9:1 (v/v) ethanol/water mixture.[27] For both the O_2 and pH sensor, the coumarin antenna dye was added to increase the brightness of the respective indicator.[35]

The respective sensing cocktails were coated onto a 125 μm thick transparent polyester foil (http://www.goodfellow.com/) using a homemade knife-coating device. The final dry thickness of the sensing layers was ∼5 and ∼20 μm for the oxygen and pH sensor, respectively. The cured sensing layers were additionally coated with a translucent thick carbon powder containing a silicone or hydrogel layer for the O_2 and pH optode, respectively. The carbon-containing layer was added to avoid wavelength-dependent scattering from roots and soil.[27]

DGT. The DGT resin gel used in the sensors was a suspended particulate reagent−iminodiacetate (SPR−IDA).[36] The SPR−IDA resin was supplied pre-cleaned as a 1 g suspension. A total of 10 mL of acrylamide (40%, BDH Electran) and 2.5 mL of DGT cross-linker (DGT Research, Ltd.) were mixed together. A total of 1 mL of this mixture was then added to 1 mL of SPR−IDA, which forms a 5% SPR−IDA gel resin solution. To this solution, 14 μL of ammonium persulfate (BDH) and 4 μL of *N,N,N,N*-tetramethylethylenediamine (TEMED, BDH Electran) were added. The gel solution was then immediately pipetted between two glass plates, where a 0.05 mm spacer was used to ensure that the solution polymerized into a gel with the desired thickness.[30] The glass plate assembly was then placed in a 45 °C oven for 1 h, after which the glass plates were separated and the resin gel was placed into 0.5 L of ultrapure water (filtered by Millipore, 18.2 MΩ) and allowed to fully hydrate for a minimum of 24 h. Prior to deployment, the resin gel was sandwiched between two acid-washed polycarbonate filter membranes (Nucleopore, Whatman, 0.4 μm pore size and 10 μm thickness). The combined thickness of the hydrated resin gel and filter membranes was 0.07 mm. The polycarbonate filter membranes served as a diffusion layer for the resin gel and protected it from direct contact with the sediment. To minimize contamination, all preparation and processing of gels was carried out in a laminar

dx.doi.org/10.1021/es501127k | Environ. Sci. Technol. 2014, 48, 8498−8506

flow class-100 clean bench within a clean room using ultraclean trace metal techniques.

Planar Optode Imaging. Two planar optode systems were applied in this study. They were previously described in detail[27,37,38] and will only be described briefly. O_2 images were recorded with a fast gateable 12-bit camera through a 590 nm long-pass filter. Excitation light was delivered from four high-power light-emitting diodes (LEDs; λ peak = 445 nm; LXHL-LR3C, Luxeon) equipped with a 470 nm short-pass filter. Recorded images were calibrated using the phosphorescent lifetime of known O_2 concentrations (saturation in the overlying water and 0% air saturation in anoxic soil), using a modified Stern–Volmer equation.[39]

The pH images were recorded using a standard digital single-lens reflex camera equipped with a 450 nm long-pass filter. Excitation light was delivered from five high-power ultraviolet (UV) LEDs (λ peak = 405 nm; LZ1-10UA05, LedEngin) equipped with a 405 nm short-pass filter. Recorded images were calibrated using the intensity ratio of the blue and red images recorded simultaneously by the camera, for known pH concentrations using a four parameter sigmoidal curve.[27]

Combination of Sensors. The planar optode foil was attached with tape (Scotch super 33+) to the inside of a transparent rhizotron and, subsequently, overlain by the ultrathin resin gel and filter layer (GFL). The backing membrane that facilitated transport was left on. The GFL was fixed on the top of the planar optode with tape (Scotch super 33+). After deployment, the GFL was rinsed with MQ water and removed from the planar optode, using a Teflon-coated razor blade and plastic forceps. It was placed immediately in a pre-cleaned sealable polythene bag, double-bagged, and stored flat at 4 °C until analysis. Before laser ablation, the GFL was mounted on a 0.04 cm thick hydrogel layer backed by a hydrated polysulfone filter membrane. The stack was left to partially air dry in a class-100 clean bench for 1 h before being placed on thick blotting paper and covered with acid and MQ-washed plastic film. Light pressure was then applied to the stacks for 12 h to enable further removal of water from the gels. Finally, the gels were transferred to a gel drier (Bio-Rad model 543) at 50 °C for 8 h. When completely dry, the gel was mounted onto glass panes (6 × 5 × 0.4 cm) with double-sided adhesive tape while maintaining the original area dimensions.[28]

Laser Ablation–ICP–MS. Thermo X series 2 ICP–MS was operated with an Xs high-sensitivity interface and Pt-tipped sampler and microskimmer cones. Calibration and detector performance were optimized prior to commencing dry plasma tuning. A Nd:YAG laser (New Wave, Cambridge, U.K.), with wavelength quadrupoled to 213 mm, was equipped with a large format ablation cell ($W \times L \times L$ = 15.24 × 15.24 × 2.54 cm). Line scans of the gels were conducted at a scanning speed of 100 μm s^{-1}, an interline spacing of 400 μm, a beam diameter of 100 μm, and a repetition rate of 20 Hz.[40] The ablation intensity was set at 50%, which equated to a fluence of 0.012 J cm^{-2}. During all runs, laser intensity and fluencies were automatically logged to monitor laser stability. ICP–MS was tuned on m/z 7, 29, 59, 89, 115, 175, and 238 by the continuous ablation of a certified reference material, National Institute of Standards and Technology (NIST) 612 glass wafer (https://www-s.nist.gov/srmors/view_detail.cfm?srm=612). In addition, oxide formation (m/z 254/238), ArOH (m/z 57), ArAr (m/z 79), and backgrounds (m/z 5 and 220) were monitored. ICP–MS was used to record ^{13}C, ^{52}Cr, ^{53}ClO, ^{55}Mn, ^{57}Fe, ^{59}Co, ^{60}Ni, ^{63}Cu, ^{65}Cu, ^{66}Zn, ^{75}As, $^{77}ArCl$, ^{82}Se, ^{83}Kr, ^{111}Cd, and ^{115}In signals; the readout time for a single reading was 0.266 s. See the Supporting Information for a summary of the element-specific limits of detection (LODs). Carbon (m/z 13) was used as an internal standard to cancel out variations in ablation, transport, and ionization efficiency. Data processing was conducted in Excel,[40] and DGT and optode images were produced in ImageJ 1.46r [National Institutes of Health (NIH), Bethesda, MD].

RESULTS

A sensor assembly with an O_2-sensitive optode was deployed with a DGT measurement window of 20 × 14 mm centered on a root tip below the soil/water interface and encompassing aerobic and anaerobic root zones (experiment 1 in Figure 2).

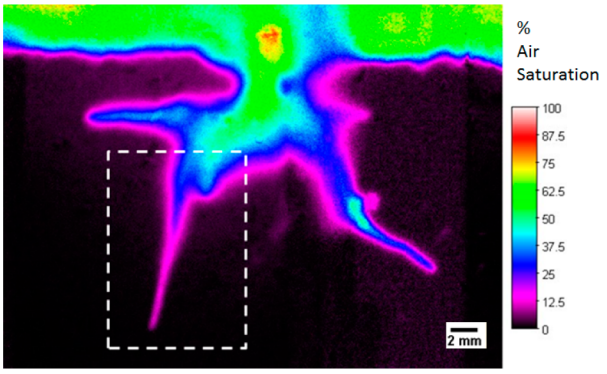

Figure 2. Oxygen distributions, imaged by a planar optode sensor, within a rice seedling rhizosphere. The O_2 level (percent air saturation) increased sequentially with the color scale shown from black to white. The outlined position of the DGT ultrathin GFL that is featured in Figure 3 is indicated by white dash markings. This image is part of 36 images recorded in series, with an interval time of 30 min.

An aerobic zone surrounding the root tip in an otherwise anoxic soil was sustained for the duration of the deployment, consistent with one-dimensional measurements of the redox potentials in rice rhizospheres.[41] Fe(II) mobilization was congruent to that of the peripheral edge of the aerobic zone (as shown in the O_2 optode image in Figure 3), demonstrating that, in our experimental conditions, the Fe(II) mobilization maximum only develops in a narrow O_2 range (7–15% air saturation) as the oxidation front penetrates the reducing soil. Averaged over the apparent root tip with sub-saturated O_2 concentrations, the Fe flux to the DGT resin was measured as 1572 ± 766 pg cm^{-2} s^{-1} (n = 50 averaged measurements, each 0.24 mm^2; Table 1), equating to a 27-fold increase in Fe availability compared to the adjacent aerobic zone and a 3-fold enhancement over that of the anaerobic bulk environment (Figure 3). These differences between zones were confirmed statistically using the Mann–Whitney test ($p < 0.0001$). Lead and As mobilization was coincidental with that of Fe(II). There was generally enhanced mobilization of Co, Ni, and Zn in the wider vicinity of the root, but this diminished where the Fe(II) release peaked (Figure 3). The DGT-measured flux is determined by the concentration adjacent to the device surface. Although this surface concentration will be modified by the DGT sink, the device cannot induce a localized maximum or minimum. Rather, localized maxima in the flux reflect localized maxima in the concentration,[42] indicating a localized process of mobilization.

dx.doi.org/10.1021/es501127k | Environ. Sci. Technol. 2014, 48, 8498–8506

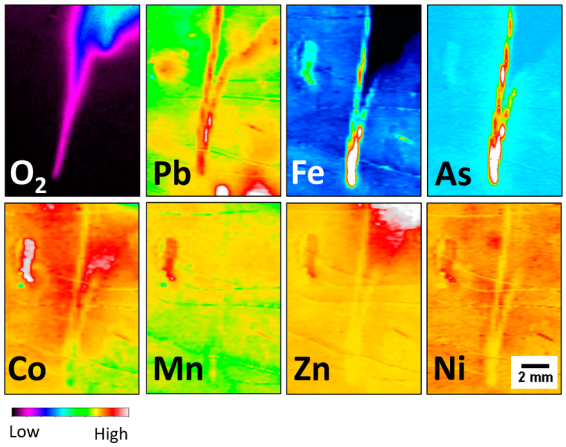

Figure 3. Visualization of O_2, Pb, Fe, As, Co, Mn, Zn, and Ni around a set of rice roots. Measurements were made by deploying an O_2 optode–DGT sensor vertically in the anoxic soil and encompassed a submerged root tip located 10 mm below the soil surface. The metal fluxes (f_{DGT}, pg cm^{-2} s^{-1}) and oxygen concentration (percent air saturation) increased sequentially with the color scale shown from blue to white. The scales in the figure represent the following ranges from 0 to 100 for O_2, from 0.15 to 0.19 for Pb, from 0.88 to 2328 for Fe, from 0.01 to 0.44 for As, from 0.05 to 0.94 for Co, from 0.43 to 173 for Mn, from 0.52 to 2.89 for Zn, and from 0.04 to 0.30 for Ni.

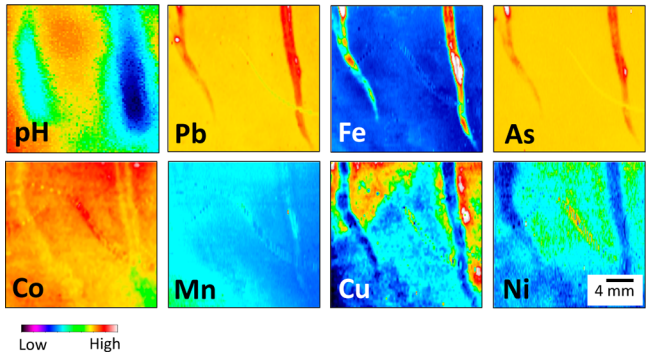

Figure 4. Two-dimensional representation of pH, Pb, Fe, As, Co, Mn, Cu, and Ni around a different set of rice root grown in the same soil at a depth of 10.5 cm from the soil–water interface. The images were obtained from a pH optode partnered with an ultrathin 0.05 mm Chelex DGT. The blue to white color scale reflects a sequential increase in metal fluxes (f_{DGT}, pg cm^{-2} s^{-1}) and pH. The scales in the figure range from 7.89 to 8.47 for pH, from 0.002 to 0.35 for Pb, from 0.8 to 261 for Fe, from 0.11 to 0.72 for As, from 0.001 to 0.12 for Co, from 0.60 to 89 for Mn, from 0.04 to 0.09 for Cu, and from 0.05 to 0.15 for Ni.

A pH-sensitive optode was partnered with DGT and deployed against a different set of rice roots (same cultivar, RIL 46) grown in the same soil (experiment 2). In contrast to the O_2 optode experiment, the rice grew for 3 weeks in the soil and, in that period, developed a deeper root system. The DGT/optode sensors were positioned 8 cm below the soil–water interface, and a similar suite of metals was measured. In agreement with the first experiment, Fe(II), As, and Pb mobilization at the rice root tips exceeded that of the bulk soil environment, while Co, Ni, and Cu were diminished (Figure 4). Planar optode measurements of pH demonstrated a localized acidification around roots of ~0.5 pH units, consistent with one- and two-dimensional observations of root-associated pH changes,[26,43,44] because metal cations are liberated from soil constituent surfaces as pH is lowered;[45] pH changes appear to be at least partially responsible for the observed metal dynamics.

Several other additional lines of evidence for root-intensified metal dynamics associated with local and pH minima O_2 leakage are available. The homogeneity of metal mobilization was interrogated on a flooded soil-packed rhizotron (experiment 3 in Figure 5). The key features of the soil system without the influence of the rice were uniform two-dimensional flux characteristics, with the overlying water reflecting higher concentrations of Pb, Zn, Cu, and Ni than in the anaerobic zone, which was typified by mobilization of Fe, As, and Co. Manganese reduction occurs at higher redox potentials than Fe, but Mn(II) is oxidized more slowly than Fe(II).[46] Figure 5 captures this process well, as evidenced by mobilization occurring immediately above the soil–water interface.

To test whether the rice root was directly affecting the metal dynamics, an experiment was conducted using an artificial root (experiment 4). An O_2 flux into anaerobic soil, mimicking that of a rice root, was achieved using 4 mm diameter silicone tubing with 1 mm thick walls (see Figure S1 of the Supporting Information). Clear Fe(II) and Pb mobilization maxima corresponded to where the oxidation front penetrated the reduced soil. Co, Ni, and Zn were also mobilized from the soil solution, as observed in the rhizosphere setup. This confirms that zones of metal depletion around rice root tips cannot be explained by plant uptake alone and suggests that simple chemical mechanisms are responsible or play a significant role (see Figure S1 of the Supporting Information). Mobilization of metals in the vicinity of O_2 can also be due to sulfide oxidation.[28] Deployments of AgI DGT probes[47] in the rhizotrons after the sandwich-probe measurements demonstrated the virtual absence of sulfide (<0.1 μM); therefore, this mode of metal mobilization is unlikely in the current setup.

Continued decomposition of organic matter under anoxic conditions requires the reoxidation of intracellular electron acceptors produced by catabolic reactions in excess of the requirements by anabolic respiration. The fervency of the reduction process largely depends upon the availability, abundance, and type of the decomposable organic compound.[48] "Hotspots" of reactive organic material are a common

Table 1. DGT Flux Measurements for Pb, Fe, As, Co, and Mn for Experiment 1[a]

	Pb	Fe	As	Co	Mn
	f_{DGT} (pg cm^{-2} s^{-1})	f_{DGT} (pg cm^{-2} s^{-1})	f_{DGT} (pg cm^{-2} s^{-1})	f_{DGT} (pg cm^{-2} s^{-1})	f_{DGT} (pg cm^{-2} s^{-1})
root tip	0.171 ± 0.002	1572 ± 766	0.38 ± 0.1	0.29 ± 0.02	28 ± 1
microniche	0.166 ± 0.001	730 ± 152	0.04 ± 0.0	0.49 ± 0.09	61 ± 16
anaerobic bulk soil	0.166 ± 0.000	578 ± 9	0.03 ± 0.0	0.33 ± 0.01	32 ± 1
aerobic rhizosphere	0.165 ± 0.000	58 ± 3	0.01 ± 0.0	0.24 ± 0.02	30 ± 1

[a]Average ± standard deviation for 50 averaged measurements, each 0.24 mm^2.

dx.doi.org/10.1021/es501127k | Environ. Sci. Technol. 2014, 48, 8498–8506

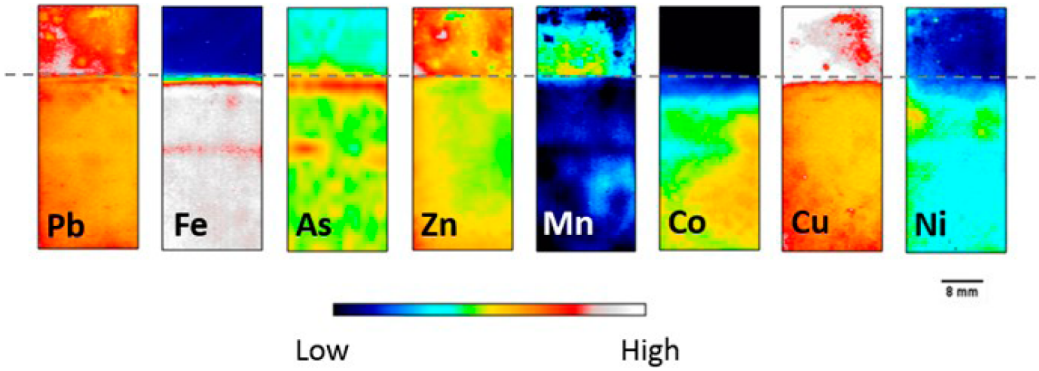

Figure 5. Characterizing the two-dimensional distributions of Pb, Fe, As, Zn, Mn, Co, Cu, and Ni in a system without a rice seedling. Deployment of a 0.4 mm DGT GFL followed the same methodology as the sandwich sensor. All other experimental features were kept the same as the planted experiments. Metal fluxes (f_{DGT}) are presented in pg cm^{-2} s^{-1}. The soil–water interface is shown by the black dashed line. The scales in the figure range from 0.20 to 0.21 for Pb, from 0.88 to 74 for Fe, from 0.01 to 0.35 for As, from 0.32 to 0.75 for Zn, from 0.001 to 0.12 for Co, from 0.38 to 76 for Mn, from 0.17 to 0.19 for Cu, and from 0.04 to 17 for Ni.

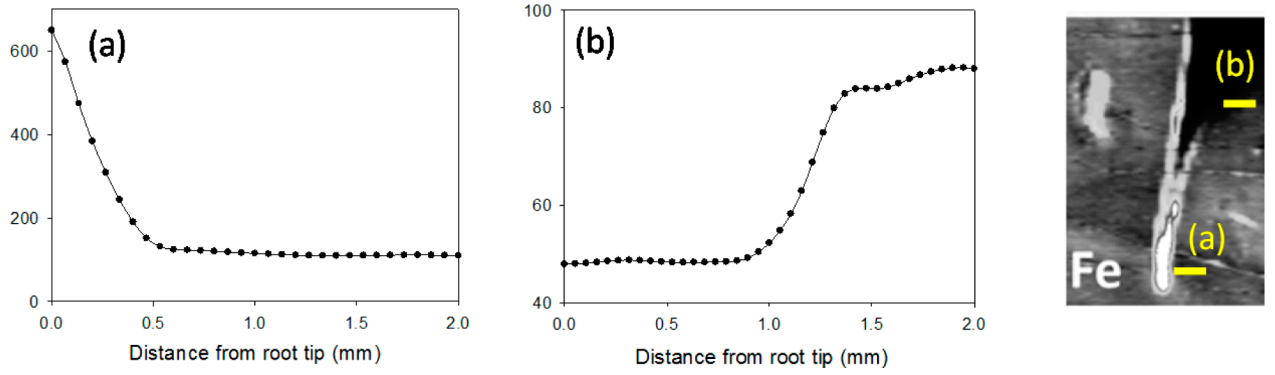

Figure 6. Fe(II) species in the soil solution with distance from the root zone. The far right inset indicates where the cross-sections (a and b) were sampled.

phenomenon in submerged soils[49] and fuel-localized, microbial-driven reductive mobilization of Fe, Mn, and associated trace metals.[48] Such a feature was observed approximately 8 mm away from the root apex (Figure 3). Fluxes of Fe and Mn in the microniche were statistically different from either the bulk soil or root tip (Mann–Whitney test; $p < 0.0001$; $n = 50$; 0.24 mm^2 averaged measurements). However, the most prominent trends were the high fluxes observed in Pb, Zn, Cu, and Ni. The elemental ratios of mobilized metals and the morphological characteristics of this microniche were similar to those observed previously for microniches[50] and distinctly different from those observed adjacent to the root, indicating their mechanistic separation (see Figure S2 of the Supporting Information).

DISCUSSION

Our findings are consistent with a series of finely poised competitive processes. The two main mechanisms to be considered are the physicochemical process of Fe(II) diffusion and its chemical oxidation. As Fe(II) diffuses from the reduced zone of submerged soil to an adjacent oxidized zone, it accumulates as precipitated Fe(III) iron; this removal of Fe from solution by oxidation is clearly visualized for the first time (Figure 3) by simultaneous DGT and optode measurements. Moving away from the core of the root zone, O_2 released by the root will have reacted mainly with *in situ* Fe(II) to form Fe(III),[22] which is not measured by DGT. As the periphery region is approached, the proportion of the Fe(III)-forming Fe(II) that has diffused into the region increases. The overall effect therefore is an enrichment of the root zone with iron; although this phenomenon has been widely observed,[8,9,12−14] its dynamics have not. By imaging the variations in solute fluxes across the root zone, a series of striking trends emerges. First, the intensity and sharpness of the Fe(II) flux maxima and its superimposition on the outer boundary of the aerobic zone is suggestive of a dominant abiotic process and supports the importance of the effect of oxidation-mediated pH changes on Fe(II) mobility. Protons are released in the Fe(II) oxidation process (eq 1), locally lowering the pH. A maximum in Fe(II) can arise because (a) its oxidation, which is very pH-sensitive, is slowed and/or (b) Fe(II) is desorbed from the freshly formed oxide.

$$4Fe^{2+} + O_2 + 6H_2O = 4FeOOH + 8H^+ \quad (1)$$

Acidification by H^+ release from roots, other efflux processes, and microbial metal release may further compound the process, but these mechanisms alone do not explain the tight association between O_2 diffusion and Fe mobility, with a similar mobility maxima being observed in the absence of a plant (see Figure S1 of the Supporting Information).

Diffusion gradients or a depletion of Fe(II) was not observed in the anaerobic bulk soil immediately adjacent to metal flux maxima (Figure 3). On the basis of models of Fe(II) diffusion toward the oxidation zone[25] and considering the microscale resolution of the measurements, a decrease in Fe(II) would have been predicted. The oxidation rate and Fe(II) resupply from the bulk soil could partially account for this, because this

dx.doi.org/10.1021/es501127k | Environ. Sci. Technol. 2014, 48, 8498−8506

would impact the net rate of oxidation and the distribution of iron species in the soil. The slower the rate, the further the oxidation front would develop and the more effectively Fe(II) diffusion would be able to match Fe(II) consumption via oxidation. A faster rate would result in smaller depletion zones, less dispersion into the soil, and hence, greater iron accumulation near the root surface. Higher Fe concentrations would give rise to a larger net rate of oxidation.[25]

The rice rhizosphere is an element sink maintained by radial O_2 loss, while adjustments to the redox equilibrium can cause localized accretions to disperse. Such variations may provide a possible explanation of what is being observed at the root tips, namely, diffusion of Fe(II) to the surrounding anaerobic soil, as indicated in Figure 6. In contrast, Figure 6 shows that, in regions of the root zone aerobic/anaerobic interface, where the Fe(II) flux maxima was not observed, there is a diffusion gradient of Fe(II) from the bulk soil toward the redox interface. In a highly dynamic system, as evident around the root apexes (Figures 3 and 4), multiple diffusion−oxidation reactions would be overlaid, with the DGT measurement providing a summation of these processes.

Rice plants immobilize trace metals in the root zone, which ensures protection from toxicity,[51] but at the same time must mine this elemental resource for essential nutrients.[12] It is in this paradox that the functionality of the dynamic and heterogeneously[9] distributed Fe plaques arises. The low Co, Ni, Cu, and Zn fluxes observed around the root tip might simply be due to competition from other sinks, i.e., plant or microbial uptake. However, given that this phenomenon only occurred specifically within the As, Pb, and Fe(II) mobilization maxima whether or not they formed in the presence of a plant, this suggests a geochemical process.

The sorption of trace metals to Fe oxides is pH-sensitive, but it is also well-established that elemental retention is in proportions that both reflect solution composition and element-specific binding properties.[45] Freshly formed oxyhydroxides act as highly reactive surfaces for rapid immobilization of trace metals by sorption, yet these most reactive phases are very amorphous and more susceptible to rapid dissolution.[22] Pb has a particularly high affinity for Fe oxide,[52] with binding constants at least an order of magnitude higher than Ni, Cu, Co, and Zn.[53,54] We hypothesize that the localized mobilization of Pb in the root zone developed because the desorptive release of Pb was faster than its concomitant removal as fresh iron oxide forms. This proportionally higher release rate for Pb would be aided by the reservoir/pool of Fe-oxide-captured Pb being greater than that of the other metals. For the metals that do not partition so strongly, namely, Co, Ni, Cu, and Zn, their pH-mediated desorptive release did not outweigh their overall removal at any point in the concentration gradient.

The co-occurrence of As and Fe flux maxima is not unexpected. Arsenic is readily retained on Fe oxides, and their release often coincides.[55] Meanwhile, with the redox threshold for the Fe(III)/Fe(II) transition lying close to the arsenate/arsenite boundary, the transformation to arsenite would favor a more rapid and extensive desorption.[19,21] Other mechanisms also are viable. Acid-soluble phosphate pools can account for 90% of the phosphate taken up in the rhizopheres of lowland rice. This includes phosphates sorbed to ferrous carbonates and hydroxides and fractions that are immobilized by Fe(II)-bridging mechanisms to negatively charged surfaces.[24] An analogous situation may also be occurring in the case of arsenic release here. Fe dissolution mechanisms could also play a role, but the time scale for this transformation would be greater. Natural organic matter (NOM) release in flooded soils can be substantial, occurring in less reducing conditions and faster than Fe(II) mobilization. NOM can promote desorption of metals and arsenic from solid phases by altering soil/solution equilibrium, both directly by binding elements via ligand-exchange reactions or mediating changes in redox conditions.[56]

Root iron plaques are a ubiquitous feature of wetland systems, forming a discontinuous precipitate that encapsulates the roots of not only rice but also many other aquatic plants. It is perhaps surprising that rice exhibits such an inclination to accumulate As and Pb if root plaques functioned solely to block metal uptake. This demonstration of mobilization of metals within the plaque provides a new perspective in understanding the supply of micronutrients and contaminants in both rice cultivation and wetland soils more generally.

■ ASSOCIATED CONTENT

Supporting Information

Soil characterization (Table S1), LODs (Table S2), artificial root experiment (Figure S1), and comparison of geochemical trends in the root tip and microniche zones (Figure S2). This material is available free of charge via the Internet at http://pubs.acs.org.

■ AUTHOR INFORMATION

Corresponding Author

*Telephone: +44-0-28-9097-6539. Fax: +44-0-28-90976513. E-mail: p.williams@qub.ac.uk.

Notes

The authors declare no competing financial interest.

■ ACKNOWLEDGMENTS

The authors gratefully acknowledge the U.K.−China Science Bridge Project funded by the Research Councils U.K. (EP/G042683/1) and the support of the Austrian Science Fund (Project P23798-B16). Ronnie N. Glud and Morten Larsen were financially supported by the Commission for Scientific Research in Greenland (KVUG, GCRC6507), the Danish National Research Foundation (DNRF53), the Danish Council for Independent Research (FNU-12-125843), and the European Research Council (ERC) Advanced Grant (ERC-2010-AdG_20100224). The authors acknowledge Matthias Wissuwa (Japan International Research Center for Agricultural Sciences, Owashi, Tsukuba, Japan) for kindly providing rice seeds. Further the authors acknowledge Richard Bardgett (University of Manchester, Manchester, U.K.) and Andrew Meharg (Queen's University Belfast, Belfast, U.K.) for constructive comments.

■ REFERENCES

(1) Williams, P. N.; Villada, A.; Deacon, C.; Raab, A.; Figuerola, J.; Green, A. J.; Feldmann, J.; Meharg, A. A. Greatly enhanced arsenic shoot assimilation in rice leads to elevated grain levels compared to wheat and barley. *Environ. Sci. Technol.* **2007**, *41*, 6854−6859.

(2) Stone, R. Food safety. Arsenic and paddy rice: A neglected cancer risk? *Science* **2008**, *321*, 184−185.

(3) Meharg, A. A.; Williams, P. N.; Deacon, C.; Sun, G.; Zhu, Y.-G.; Feldmann, J.; Raab, A.; Zhao, F.-J.; Hossain, S. Geographical variation in total and inorganic arsenic content of polished (white) rice. *Environ. Sci. Technol.* **2009**, *43*, 1612−1617.

(4) Norton, G.; Williams, P. N.; Adomako, E. E.; Price, A.; Zhu, Y.-G.; Zhao, F.-J.; McGrath, S.; Deacon, C.; Villada, A.; Sommella, A.; Lu, Y.; De Silva, M. S. S.; Brammer, H.; Dasgupta, T.; Islam, M. R.; Meharg, A. A. Lead in rice: Analysis of baseline lead levels in market and field collected rice grains. *Sci. Total Environ.* **2014**, *485*, 428−434.
(5) Institute for Health Metrics and Evaluation (IHME). *Global Burden of Disease (GBD)*; http://www.healthdata.org/gbd.
(6) Welch, R. M.; Graham, R. D. Breeding for micronutrients in staple food crops from a human nutrition perspective. *J. Exp. Bot.* **2004**, *55*, 353−364.
(7) Doberman, A.; Fairhurst, T. H. *Rice Nutrient Disorders and Nutrient Management*; International Rice Research Institute: Los Baños, Laguna, Philippines, 2000.
(8) Chen, C. C.; Dixon, J. B.; Turner, F. T. Iron coatings on rice roots: Morphology and models of development. *Soil Sci. Soc. Am. J.* **1980**, *44*, 1113−1119.
(9) Seyfferth, A. L.; Webb, S. M.; Andrews, J. C.; Fendorf, S. Arsenic localization, speciation, and co-occurrence with iron on rice (*Oryza sativa* L.) roots having variable Fe coatings. *Environ. Sci. Technol.* **2010**, *44*, 8108−8113.
(10) Liu, W. J.; Zhu, Y. G.; Hu, Y.; Williams, P. N.; Gault, A. G.; Meharg, A. A.; Charnock, J. M.; Smith, F. A. Arsenic sequestration in iron plaque, its accumulation and speciation in mature rice plants (*Oryza sativa* L.). *Environ. Sci. Technol.* **2006**, *40*, 5730−5736.
(11) Kuo, S. Concurrent sorption of phosphate and zinc, cadmium, or calcium by a hydrous ferric oxide. *Soil Sci. Soc. Am. J.* **1986**, *50*, 1412−1419.
(12) Greipsson, S.; Crowder, A. A. Amelioration of copper and nickel toxicity by iron plaque on roots of rice (*Oryza sativa*). *Can. J. Bot.* **1992**, *70*, 824−830.
(13) Christensen, K. K.; Jensen, H. S.; Andersen, F. O.; Wigand, C.; Holmer, M. Interference between root plaque formation and phosphorus availability for isoetids in sediments of oligotropic lakes. *Biogeochemistry* **1998**, *4*, 107−128.
(14) Batty, L. The effect of pH and plaque on the uptake of Cu and Mn in *Phragmites australis* (Cav.) Trin ex. Steudel. *Ann. Bot.* **2000**, *86*, 647−653.
(15) Ye, Z. H.; Cheung, K. C.; Wong, M. H. Copper uptake in *Typha latifolia* as affected by iron and manganese plaque on the root surface. *Can. J. Bot.* **2001**, *79*, 314−320.
(16) Schmidt, H.; Eickhorst, T.; Tippkötter, R. Monitoring of root growth and redox conditions in paddy soil rhizotrons by redox electrodes and image analysis. *Plant Soil* **2010**, *341*, 221−232.
(17) Reddy, K. R.; Patrick, W. H. Effect of frequent changes in aerobic and anaerobic conditions on redox potential and nitrogen loss in a flooded soil. *Soil Biol. Biochem.* **1976**, *8*, 491−495.
(18) Masscheleyn, P. H.; Delaune, R. D.; Patrick, W. H. Effect of redox potential and pH on arsenic speciation and solubility in a contaminated soil. *Environ. Sci. Technol.* **1991**, *25*, 1414−1419.
(19) Takahashi, Y.; Minamikawa, R.; Hattori, K. H.; Kurishima, K.; Kihou, N.; Yuita, K. Arsenic behavior in paddy fields during the cycle of flooded and non-flooded periods. *Environ. Sci. Technol.* **2004**, *38*, 1038−1044.
(20) Xu, X. Y.; McGrath, S. P.; Meharg, A. A.; Zhao, F. J. Growing rice aerobically markedly decreases arsenic accumulation. *Environ. Sci. Technol.* **2008**, *42*, 5574−5579.
(21) Yamaguchi, N.; Nakamura, T.; Dong, D.; Takahashi, Y.; Amachi, S.; Makino, T. Arsenic release from flooded paddy soils is influenced by speciation, Eh, pH, and iron dissolution. *Chemosphere* **2011**, *83*, 925−932.
(22) Kirk, G. *The Biogeochemistry of Submerged Soils*; John Wiley and Sons: Hoboken, NJ, 2004.
(23) Walker, T. S.; Bais, H. P.; Grotewold, E.; Vivanco, J. M. Root exudation and rhizosphere biology. *Plant physiol.* **2003**, *132*, 44−51.
(24) Saleque, M. A.; Kirk, G. J. D. Root-induced solubilization of phosphate in the rhizosphere of lowland rice. *New Phytol.* **1995**, *129*, 325−336.
(25) Kirk, G. J. D.; Ahmad, A. R.; Nye, P. H. Coupled diffusion and oxidation of ferrous iron in soils. II. A model of the diffusion and reaction of O_2, Fe^{2+}, H^+ and HCO_3^- in soils and a sensitivity analysis of the model. *J. Soil Sci.* **1990**, *41*, 411−431.
(26) Begg, C. B. M.; Kirk, G. J. D.; Mackenzie, A. F.; Neue, H.-U. Root-induced iron oxidation and pH changes in the lowland rice rhizosphere. *New Phytol.* **1994**, *128*, 469−477.
(27) Larsen, M. S.; Borisov, M.; Grunwald, B.; Klimant, I.; Glud, R. N. A simple and inexpensive high resolution color ratiometric planar optode imaging approach: Application to oxygen and pH sensing. *Limnol. Oceanogr.: Methods* **2011**, *9*, 348−360.
(28) Stahl, H.; Warnken, K. W.; Sochaczewski, L.; Glud, R. N.; Davison, W.; Zhang, H. A combined sensor for simultaneous high resolution 2-D imaging of oxygen and trace metals fluxes. *Limnol. Oceanogr.: Methods* **2012**, *10*, 389−401.
(29) Santner, J.; Zhang, H.; Leitner, D.; Schnepf, A.; Prohaska, T.; Puschenreiter, M.; Wenzel, W. W. High-resolution chemical imaging of labile phosphorus in the rhizosphere of *Brassica napus* L. cultivars. *Environ. Exp. Bot.* **2012**, *77*, 219−226.
(30) Lehto, N. J.; Davison, W.; Zhang, H. The use of ultra-thin diffusive gradient in thin-films (DGT) devices for the analysis of trace metal dynamics in soils and sediments: A measurement and modelling approach. *Environ. Chem.* **2012**, *9*, 415−423.
(31) Tipping, E. Humic ion-binding model VI: An improved description of the interactions of protons and metal ions with humic substances. *Aquat. Geochem.* **1998**, *4*, 3−47.
(32) Rau, I.; Gonzalo, A.; Valiente, M. Arsenic(V) adsorption by immobilized iron mediation. Modeling of the adsorption process and influence of interfering anions. *React. Funct. Polym.* **2003**, *54*, 85−94.
(33) Borisov, S. M.; Klimant, I. Luminescent nanobeads for optical sensing and imaging of dissolved oxygen. *Microchim. Acta* **2008**, *164*, 7−15.
(34) Zhu, Q.; Aller, R. C.; Fan, Y. Two-dimensional pH distributions and dynamics in bioturbated marine sediments. *Geochim. Cosmochim. Acta* **2006**, *70*, 4933−4949.
(35) Mayr, T.; Borisov, S. M.; Abel, T.; Enko, B.; Waich, K.; Mistlberger, G.; Klimant, I. Light harvesting as a simple and versatile way to enhance brightness of luminescent sensors. *Anal. Chem.* **2009**, *81*, 6541−6545.
(36) Warnken, K. W.; Zhang, H.; Davison, W. Performance characteristics of suspended particulate reagent−iminodiacetate as a binding agent for diffusive gradients in thin films. *Anal. Chim. Acta* **2004**, *508*, 41−51.
(37) Frederiksen, M. S.; Glud, R. N. Oxygen dynamics in the rhizosphere of *Zostera marina*: A two-dimensional planar optode study. *Limnol. Oceanogr.* **2006**, *51*, 1072−1083.
(38) Holst, G.; Grunwald, B. Luminescence lifetime imaging with transparent oxygen optodes. *Sens. Actuators, B* **2001**, *74*, 78−90.
(39) Klimant, I.; Meyer, V.; Kuhl, M. Fiber-optic oxygen microsensors, a new tool in aquatic biology. *Limnol. Oceanogr.* **1995**, *40*, 1159−1165.
(40) Santner, J.; Prohaska, T.; Luo, J.; Zhang, H. Ferrihydrite containing gel for chemical imaging of labile phosphate species in sediments and soils using diffusive gradients in thin films. *Anal. Chem.* **2010**, *82*, 7668−7674.
(41) Flessa, H.; Fischer, W. R. Plant-induced changes in the redox potentials of rice rhizospheres. *Plant Soil* **1992**, *143*, 55−60.
(42) Sochaczewski, L.; Davison, W.; Zhang, H.; Tych, W. Understanding small-scale features in DGT measurements in sediments. *Environ. Chem.* **2009**, *6*, 477−485.
(43) Revsbech, N. P.; Pedersen, O.; Reichardt, W.; Briones, A. Microsensor analysis of oxygen and pH in the rice rhizosphere under field and laboratory conditions. *Biol. Fertil. Soils* **1999**, *29*, 379−385.
(44) Blossfeld, S.; Gansert, D. A novel non-invasive optical method for quantitative visualization of pH dynamics in the rhizosphere of plants. *Plant. Cell Environ.* **2007**, *30*, 176−186.
(45) Bradl, H. B. Adsorption of heavy metal ions on soils and soils constituents. *J. Colloid Interface Sci.* **2004**, *277*, 1−18.
(46) Davison, W. Iron and manganese in lakes. *Earth-Sci. Rev.* **1993**, *34*, 119−163.

(47) Widerlund, A.; Davison, W. Size and density distribution of sulfide-producing microniches in lake sediments. *Environ. Sci. Technol.* **2007**, *41*, 8044−8049.
(48) Inubushi, K.; Wada, H.; Takai, Y. Easily decomposable organic matter in paddy soils (IV): Relationship between reduction process and organic matter decomposition. *Soil Sci. Plant Nutr.* **1984**, *30*, 189−198.
(49) Stockdale, A.; Davison, W.; Zhang, H. Micro-scale biogeochemical heterogeneity in sediments: A review of available technology and observed evidence. *Earth-Sci. Rev.* **2009**, *92*, 81−97.
(50) Fones, G. R.; Davison, W.; Hamilton-Taylor, J. The fine-scale remobilization of metals in the surface sediment of the north-east Atlantic. *Cont. Shelf Res.* **2004**, *24*, 1485−1504.
(51) Tanaka, A.; Loe, R.; Navasero, S. A. Some mechanisms involved in the development of iron toxicity symptoms in the rice plant. *Soil Sci. Plant Nutr.* **1996**, *12*, 32−38.
(52) Liu, C.; Huang, P. M. Kinetics of lead adsorption by iron oxides formed under the influence of citrate. *Geochim. Cosmochim. Acta* **2003**, *67*, 1045−1054.
(53) Ponthieu, M.; Juillot, F.; Hiemstra, T.; van Riemsdijk, W. H.; Benedetti, M. F. Metal ion binding to iron oxides. *Geochem. Cosmochim. Acta* **2006**, *70*, 2679−2698.
(54) Allison, J. D.; Allison, T. L. *Partition Coefficients for Metals in Surface Water, Soil and Waste*; United States Environmental Protection Agency (U.S. EPA): Washington, D.C., 2005; EPA/600/R-05/074.
(55) Manning, B. A.; Fendorf, S. E.; Goldberg, S. Surface structures and stability of arsenic(III) on goethite: Spectroscopic evidence for inner-sphere complexes. *Environ. Sci. Technol.* **1998**, *32*, 2383−2388.
(56) Williams, P. N.; Zhang, H.; Davison, W.; Meharg, A. A.; Hossain, M.; Norton, G. J.; Brammer, H.; Islam, M. R. Organic matter−solid phase interactions are critical for predicting arsenic release and plant uptake in Bangladesh paddy soils. *Environ. Sci. Technol.* **2011**, *45*, 6080−6087.